D/H AND NEARBY INTERSTELLAR CLOUD STRUCTURES

J.L. LINSKY[1]
[1] *JILA, University of Colorado and N.I.S.T., Boulder Colorado 80309-0440, U.S.A.* (`jlinsky@jila.colorado.edu`)

Received ; accepted

Abstract. Analysis of UV spectra obtained with the HST, FUSE and other satellites provides a new understanding of the deuterium abundance in the local region of the Galactic disk. The wide range of gas-phase D/H measurements obtained outside of the Local Bubble can now be explained as due to different amounts of deuterium depletion on carbonaceous grains. The total D/H ratio including deuterium in the gas and dust phases is at least 23 parts per million of hydrogen, which is providing a challenge to models of Galactic chemical evolution. Analysis of HST and ground-based spectra of many lines of sight to stars within the Local Bubble have identified interstellar velocity components that are consistent with more than 15 velocity vectors. We have identified the structures of 15 nearby warm interstellar clouds on the basis of these velocity vectors and common temperatures and depletions. We estimate the distances and masses of these clouds and compare their locations with cold interstellar clouds.

Keywords: ISM: deuterium, abundances, structure, Ultraviolet:ISM

1. Introduction

High-resolution ultraviolet spectra provide critically important information on the chemical composition, kinematics, and physical properties of astrophysical plasmas. Many important spectral lines from a wide range of ions in the 1200–3000 Å spectral region are observable with the Goddard High Resolution Spectrograph (GHRS) and the Space Telescope Imaging Spectrograph (STIS) instruments on the Hubble Space Telescope (HST). Other ions can be studied in the 912–1200 Å region with the Far Ultraviolet Spectrograph Explorer (FUSE) satellite. I will summarize recent work in two areas based on these HST and FUSE data. The first topic is the abundance of deuterium in the Galaxy, based on observations of the Lyman lines of hydrogen and deuterium. The second topic is the structure and chemical composition of warm clouds in the nearby interstellar medium (ISM), based primarily on HST observations of resonance lines of Mg II, Fe II, and D I, together with ground-based observations of Ca II. In many cases, the same spectra provided valuable input for both topics.

2. The Abundance of Deuterium in the Galaxy

Accurate measurements of the deuterium/hydrogen (D/H) ratio (by number) provide critically important tests for models of primordial nucleosynthesis, Galactic chemical evolution, and the chemical properties of the intergalactic medium (IGM). Primordial nucleosynthesis is the only significant source of D, which is easily converted to heavier nuclei in stellar interiors before supernovae and stellar winds disperse the deuterium-poor gas into the ISM. As a result, measurements of the D abundances in different regions of the Galaxy provide a major test of Galactic chemical evolution models. Unexpectedly, our studies of D have also provided information on the composition of interstellar dust grains.

Linsky et al. (2006) summarize the recent D/H measurements and provide a model for their interpretation. Figure 1 shows the hydrogen Lyman-α line emission line from the nearby star Capella with superimposed absorption by interstellar H and D (at -0.33 Å or -82 km s^{-1} from the H line). This GHRS spectrum is typical for short lines of sight toward late-type stars with Lyman-α emission lines, but for longer lines of sight the targets are typically O stars, OB subdwarfs, and hot white dwarfs that have interstellar absorption lines superimposed on stellar Lyman-α absorption lines. Since the interstellar H absorption is a factor of 10^5 times stronger than for D, the difficult part of the analysis is to measure accurately the H column density, N(H I), from the steeply-rising flux just outside of the saturated line core. High spectral resolution is required to accurately measure the slope of the absoption. For more distant lines of sight, the H line broadens with increasing N(H I) to cover the D line, thereby forming an effective horizon for Lyman-α D/H measurements when log N(H I) ≥ 18.7.

For lines of sight with larger column densities, one must observe the less opaque higher Lyman lines, which lie in the 912–1025 Å spectral region not accessible to HST but observable with FUSE. Figure 2 shows examples of FUSE spectra of two sdO stars. The ability to study a range of Lyman lines with very different opacities allows one to infer D/H from measured N(H I) and N(D I) column densities despite line saturation, weak D I lines, or overlaping lines of H_2 and other species.

Figure 3 shows D/H measurements (and their 1σ errors) for all 47 lines of sight (Linsky et al. 2006). It is essential to recognize that the N(D I)/N(H I) ratio measures D/H only in the gas phase, $(D/H)_{gas}$. Inside the Local Bubble (log N(H I) < 19.2), which extends to roughly 100 pc from the Sun, the 22 lines of sight are consistent with a constant value of $(D/H)_{gas} = 15.6 \pm 0.4$ ppm (parts per million of H I atoms). For larger N(H I) there is a wide range of $(D/H)_{gas}$ values with a tendency to low values at log N(H I) > 20.7. This large range in $(D/H)_{gas}$ must be real as it has been found from analysis of FUSE, Copernicus, and IMAPS spectra by different authors using different

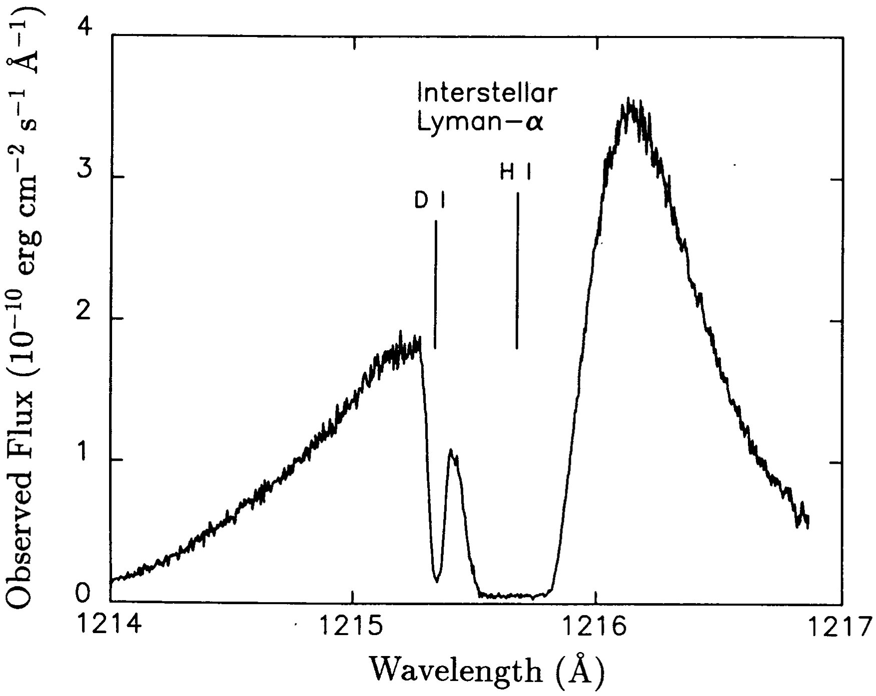

Figure 1. GHRS echelle spectrum of the star Capella (12.9 pc) showing interstellar Lyman-α absorption of H and D. Log N(H I) = 18.24. (From Linsky et al. 1995.)

analysis codes. Since a factor of four range in D/H within a few hundred parsecs of the Sun is inconsistent with existing Galactic chemical evolution models for a sensible range of assumptions (e.g., Romano et al. 2006), a new approach is necessary for understanding these data.

Developing an idea first proposed by Jura (1982), Draine (2003, 2006) showed that D could be depleted onto carbonaceous dust grains in the ISM. Since the C-D bond is 0.083 eV larger than the C-H bond, D can replace H in these grains. In thermodynamic equilibrium, $(D/H)_{\rm dust}/(D/H)_{\rm gas} \approx e^{970/T_{\rm dust}}$, which exceeds 5×10^5 for $T_{\rm dust} < 90$ K. Since interstellar dust is very cold, typically $T_{\rm dust} \sim 20$ K (Draine 2003), very high levels of deuteration are possible in carbonaceous grains and likely also in interstellar polycyclic aromatic hydrocarbon molecules. Since $(C/H)_{\rm dust} \approx 230$ ppm (Savage & Sembach 1996), under these conditions essentially all of the D could be removed from the gas phase by binding onto only 10% of the C in grains. However, the ISM is not in thermodynamic equilibrium, but rather is highly dynamic. Draine (2006) estimates that the time scale for D depletion onto grains is about 2 Myr for cold neutral clouds and about 50 Myr for

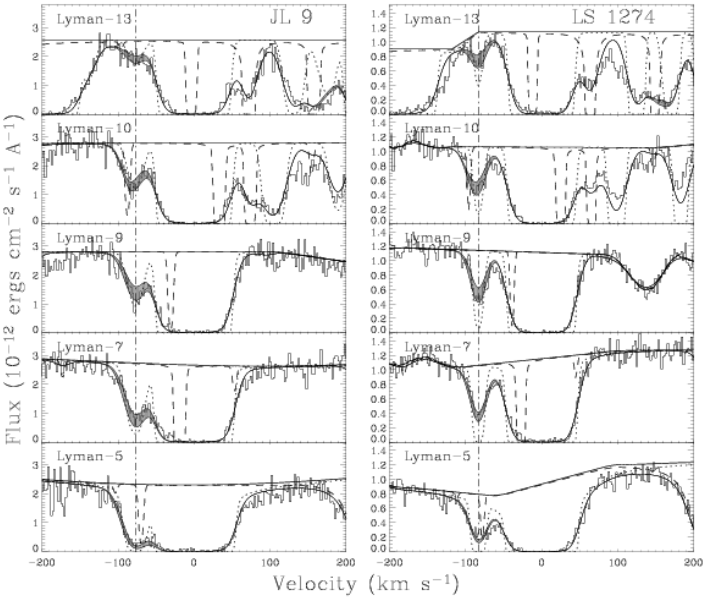

Figure 2. FUSE spectra of two hot sdO stars, JL 9 and LSS 1274, both at a distance of about 600 pc. The data are for the Lyman-5 through Lyman-13 lines. Dashed lines indicate H_2 absorption, dotted lines show the absorption due to all other lines, and solid lines show the convolution with the instrument profile. The values of log N(H I) are 20.78 and 20.98, respectively. (From Wood et al. 2004).

the warm neutral medium. Linsky et al. (2006) proposed a time-dependent D depletion model in which D is depleted when the interstellar gas remains undisturbed for some time, but the D in the dust returns to the gas phase when the dust is vaporized by shock waves or comes near hot stars.

Linsky et al. (2006) tested this model in several ways. First, they noted that Keller et al. (2000) found that carbon-rich interplanetary dust particles (IDPs) contain inclusions with D/H as high as 16,500 ppm. Since IDPs are either interstellar in origin or formed in the early solar system where conditions were similar to cold neutral clouds in the ISM, these very high D/H ratios provide a proof of concept that D can be highly depleted onto interstellar dust grains. Second, when conditions are appropriate for D depletion, other elements, especially refractory elements like iron and silicon, should also be depleted. Thus low values of $(D/H)_{gas}$ should correlate with large depletions of iron and silicon. Figure 4 shows that there is indeed a good correlation in which the Spearman test rejects no correlation at 99.8% (2.9σ). There are, however, five high points, that could be explained if D is

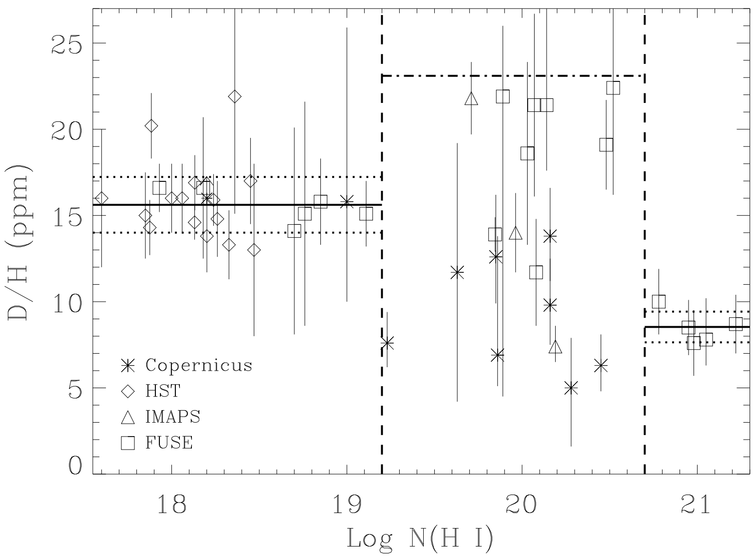

Figure 3. Plot of the gas-phase D/H values (not corrected for the Local Bubble foreground) vs. the hydrogen column density N(H I) for the 47 lines of sight studied by Linsky et al. (2006). The symbols for each data point indicate the spacecraft that observed the line of sight. Error bars are $\pm 1\ \sigma$. Vertical dashed lines indicate lines of sight inside the Local Bubble [$\log N$(H I) < 19.2 cm^{-2}] and the intermediate region [$\log N$(H I) between 19.2 and 20.7]. The solid horizontal lines indicate the mean values of $(\mathrm{D/H})_{\mathrm{gas}}$ for the low and high N(H I) regions, and the dotted horizontal lines indicate the $\pm 1\ \sigma$ errors about the mean value. The dash-dot horizontal line is the mean value of $(\mathrm{D/H})_{\mathrm{gas-LB}}$ for the highest five points in the intermediate region (γ^2 Vel, Lan 23, WD 1034+001, Feige 110, and LSE 44) after subtracting the foreground Local Bubble contributions to the hydrogen and deuterium column densities along the lines of sight.

mainly in the outer surfaces of grains that have more refractory cores. In this case, moderate strength shocks could vaporize the outer regions of the grains leaving the iron cores intact. Alternatively, there could be a low percentage of C grains in these lines of sight. A similar plot for silicon (Figure 5) also shows a correlation of $(\mathrm{D/H})_{\mathrm{gas}}$ with the depletion of Si.

If depletion is the cause of low values of the $(\mathrm{D/H})_{\mathrm{gas}}$ ratio, then according to the time-dependent D depletion model, those lines of sight with the highest measured $(\mathrm{D/H})_{\mathrm{gas}}$ values should provide a good approximation to the total (D/H) ratio in the local region of the Galactic disk, $(\mathrm{D/H})_{\mathrm{LDtotal}}$. Beyond the Local Bubble, Linsky et al. (2006) identify five lines of sight (toward γ^2 Vel, Lan 23, WD 1034+001, PG 0038+199, and TD1 32709) with the highest $(\mathrm{D/H})_{\mathrm{gas}}$ ratios. The mean value for these five lines of sight

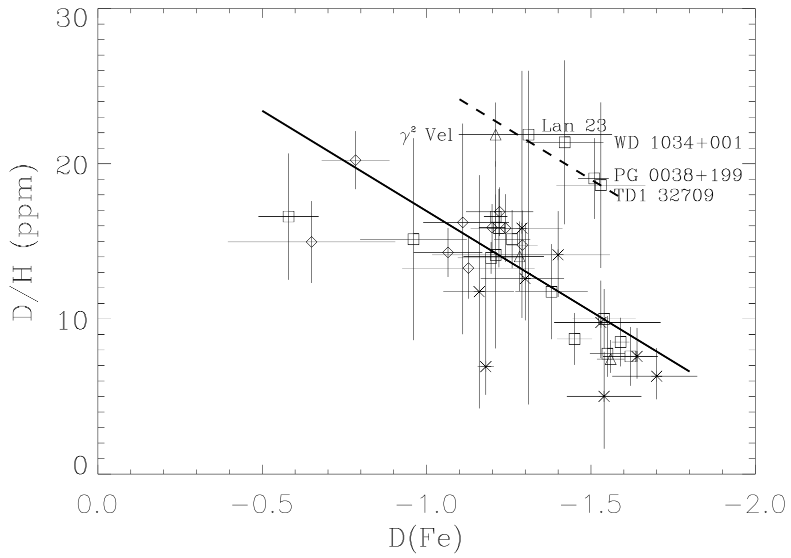

Figure 4. Plot of gas-phase D/H values in the lines of sight toward stars vs. the depletion (log units) of iron for 38 lines of sight. The symbols are the same as in Figure 3, and the error bars are $\pm 1\ \sigma$. The solid line is the least-squares linear fit to the data weighted by the inverse errors. See Linsky et al. (2006) for a discussion of the error analysis technique. Five lines of sight with $(D/H)_{gas}$ well above the linear fit are identified. The arbitrary dashed line has the same slope as the solid line but is displaced upward by 8.5 ppm.

is $(D/H)_{gas} = 21.7 \pm 1.7$ ppm. However, when the Local Bubble foreground values of N(H I) and N(D I) are subtracted, we find that $(D/H)_{LDtotal} \geq 23.1 \pm 2.4$ ppm. The $\geq$ symbol reminds us that even for the high lines of sight, some D may still be locked up in the grains.

Until recently, Galactic chemical evolution models (e.g., Romano et al. 2003) assumed that $(D/H)_{LDtotal} \approx 15$ ppm, the value of $(D/H)_{gas}$ inside the Local Bubble. However this region was shocked by supernova events several million years ago (Berghöfer & Breitschwerdt 2002) and D is no longer entirely in the gas phase. When the Galaxy was two-thirds its present age, the protosolar value of the total D/H ratio was 20 ± 3.5 ppm (Geiss & Gloeckler 2003). The deuterium astration factor is the ratio of the total D/H ratios in the primative and present-day Galaxy, $f_D = (D/H)_{prim}/(D/H)_{LDtotal}$. If one adopts the primordial (D/H) ratio infered from WMAP data (Spergel 2003), then $f_D \leq (27.5 \pm 2.1\,\mathrm{ppm})/(23.1 \pm 2.4\,\mathrm{ppm}) \leq 1.19 \pm 0.16$. If instead, one adopts the primordial ratio from Coc et al. (2004), which is based on the WMAP data but with different assumed nuclear reaction rates, then

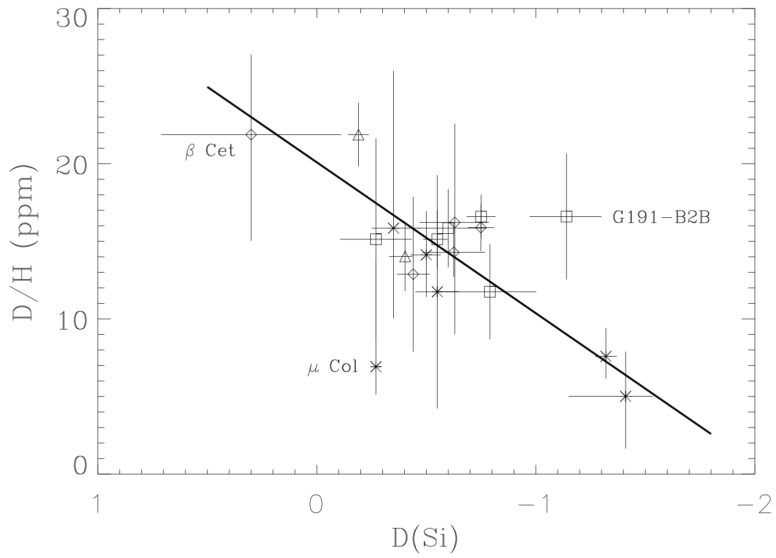

Figure 5. Plot of gas-phase D/H values in the lines of sight toward stars vs. the depletion (log units) of silicon for 20 lines of sight. The symbols are the same as in Figure 3, and the error bars are $\pm 1\ \sigma$. The solid line is the least-squares linear fit to the data weighted by the inverse errors. Four of the five high points in Figure 4 do not have Si data.

$f_{\rm D} \leq 1.12 \pm 0.14$. These very small astration factors challenge the most recent Galactic chemical evolution models. For example, the smallest astration factor in models for the Sun's distance from the Galactic Center computed by Romano et al. (2006) is $f_{\rm D} \approx 1.39$. The new value of $({\rm D/H})_{\rm LDtotal}$ will lead to a re-examination of the many assumptions that enter the chemical model calculations, in particular the infall rate and timing of D-rich and metal-poor gas from the Galactic halo and IGM.

3. Structure of the Local ISM

Seth Redfield and I are studying the properties of interstellar gas inside the Local Bubble. Our initial goal was to study the kinematics and physical properties of warm gas near the Sun using high-resolution GHRS and STIS spectra and ground-based Ca II spectra. As this work has proceeded, we have found interesting connections between the warm gas clouds and both cold gas and the locations of interstellar scintillation screens.

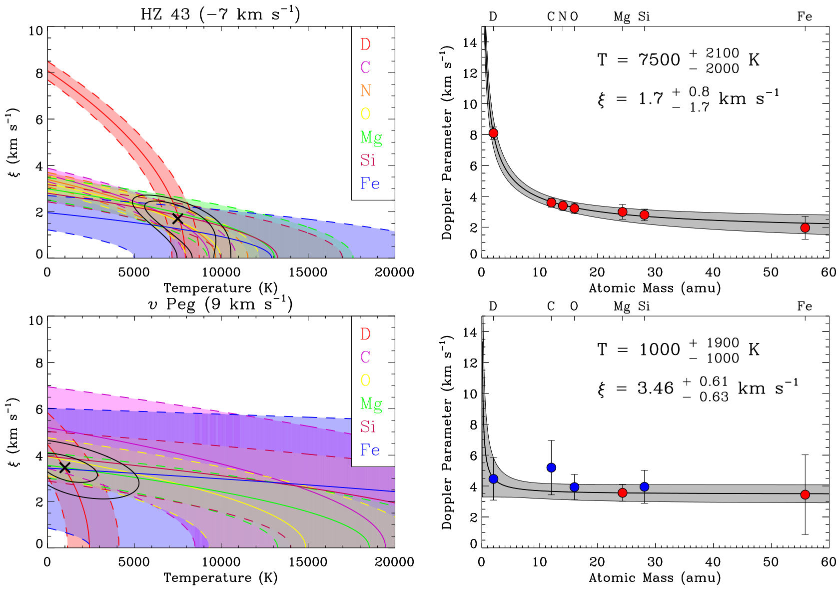

Figure 6. Technique for measuring cloud temperatures (T) and nonthermal broadening parameters (ξ) from interstellar absorption line widths. Examples are given for the –7 km s^{-1} velocity component toward HZ 43 (top panels) and the +9 km s^{-1} velocity component toward υ Peg (bottom panels). The right side panels show the Doppler line widths for atoms or ions of different atomic mass, the best fit parameters, and their $\pm 1\sigma$ errors. The left side panels show the acceptable range of T and ξ for each atom or ion and the best fit, 1σ, and 2σ range for these parameters. Figure from Redfield & Linsky 2004).

Lallement & Bertin (1992) found that the radial velocities of interstellar warm gas in the lines of sight to nearby stars can be fit with two velocity vectors, one for the Galactic Center hemisphere and the other for the anticenter hemisphere. These kinematic data permitted them to identify two warm gas clouds near the Sun, which they called the AG and G clouds, respectively. The AG Cloud is now called the Local Interstellar Cloud (LIC). Subsequently, Frisch, Grodnicki, & Welty (2002) also used kinematics to identify 7 clouds in the solar neighborhood.

Redfield & Linsky (2007) are extending this work by analysis of 146 interstellar velocity components identified in STIS and GHRS spectra of lines of sight to stars inside the Local Bubble and an additional 86 velocity components seen in ground-based Ca II spectra. We identify the shapes of clouds from common kinematic and physical properties. We first identify a cloud on the basis that the interstellar absorption line velocity components for lines of sight in the same region of the sky fit the same emprically determined flow vector to within the velocity measurement errors. In addition, we require that the interstellar gas temperatures, when available from the UV spectra, have similar values. Figure 6 shows how the temperature (T), which is best determined from D, and nonthermal broadening parameter (ξ), which is best determined from Fe, can be inferred from the measured line widths of ions with different atomic mass. UV spectra are needed to sample both light and heavy mass ions. The figure shows examples for a typical warm cloud (toward HZ 43) and a rather cool cloud (toward υ Peg).

We have now identified 15 warm clouds lying within 15 pc of the Sun. Upper limits to the cloud distances are determined from the closest star that shows interstellar absorption at the projected velocity of the cloud flow vector. Aside from the LIC, the closest warm cloud is the G Cloud seen toward α Cen (1.3 pc). Where these clouds are located along the line of sight to the nearest star is presently unknown. The cloud temperatures range from 1700 K (Oph Cloud) to about 10,000 K (Mic and Vel Clouds). The number of lines of sight used to determine the flow vectors range from 78 (for the LIC) and 21 (for the G Cloud) down to 4–6 in a few cases.

Figure 7 shows the shape of the LIC delineated by the solid line that includes all lines of sight consistent with the LIC flow vector and excludes all lines of sight inconsistent with the vector. Although the LIC is centered on the antigalactic center direction, its shape is irregular like most of the identified clouds. Since no absorption consistent with the LIC vector is seen in half of the sky, including the direction toward the nearest star (α Cen, l=315.7°, b=–0.7°), the Sun must be either just inside or just outside of the LIC. In fact, the Sun is located just inside the LIC because interstellar neutral helium gas, with a trajectory not deviated by charge exchange or ionization, flows inside the heliosphere with the LIC velocity. However the Sun is travelling at 26 km s^{-1} relative to the LIC upwind direction and will leave the LIC in less than a few thousand years.

The Sun is travelling toward the G Cloud shown in Figure 8. This cloud is somewhat cooler than the LIC (5,500 K compared with 7,500 K). The G Cloud has a more irregular shape than the LIC, and several of the 15 clouds clearly show filamentary structure. A good example is the Mic Cloud (Figure 9), which extends from the South Galactic Pole to nearly the North Pole but is very narrow. The high temperature and filamentary shape of the cloud suggests that it may be a shock front.

Now that we have some information on the location of warm gas clouds in the local ISM, we can study how the warm clouds may be related to other structures and phenomena in the local ISM. Heiles and Troland (2003) identified the Triad Region Cloud consisting of cold neutral medium (CNM) gas on the basis of H I 21 cm absorption. Centered at l=225° and b=+45°, this cloud extends over some 20 degrees in Galactic longitude and has an H I spin temperature of about 25 K. High-resolution interstellar Na I absorption

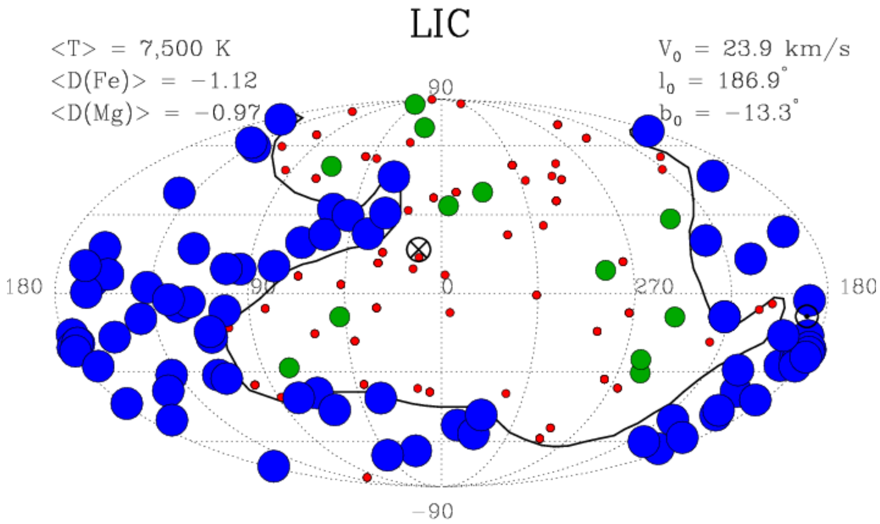

Figure 7. Outline of the Local Interstellar Cloud (LIC) in Galactic coordinates. Large dots indicate lines of sight containing velocity components consistent with the LIC velocity vector. Small dots are lines of sight with no components consistent with the LIC vector. Medium size dots indicate lines of sight that have similar kinematics to the LIC but are excluded for other reasons. The mean temperature and iron and magnesium depletions are listed in the upper left corner. The amplitude and downwind direction of the heliocentric LIC velocity vector are shown in the upper right corner. The upwind direction of the flow vector is indicated by the $\otimes$ symbol, and the downwind direction by the $\odot$ symbol.

measurements by Meyer et al. (2006) confirm the low temperature of the cloud and show that its distance must be less than 45 pc on the basis of the closest star showing the cloud's absorption. It is interesting that this cloud lies at the edge of several warm clouds. In the McKee & Ostriker (1977) model of the ISM, CNM clouds must be surrounded by warm clouds to provide shielding from ionizing radiation. Also, Vázquez-Semadeni et al. (2006) argue that CNM clouds could be formed by transonic compression of colliding warm clouds. Further study of the topological relation of cold and warm gas is possible with the Redfield & Linsky (2007) data set.

Several pulsars and quasars with very small angular diameters show large amplitude radio flux variations on time scales of hours to months, which have been interpreted as scintillation produced by turbulent interstellar gas. In some cases the distance to the scattering screen has been determined from the scintillation time scales and observations by widely separated radio telescopes. Perhaps the best example is the quasar J1819+3845 studied by Dennett-Thorpe & de Bruyn (2003), who now argue (de Bruyn, private

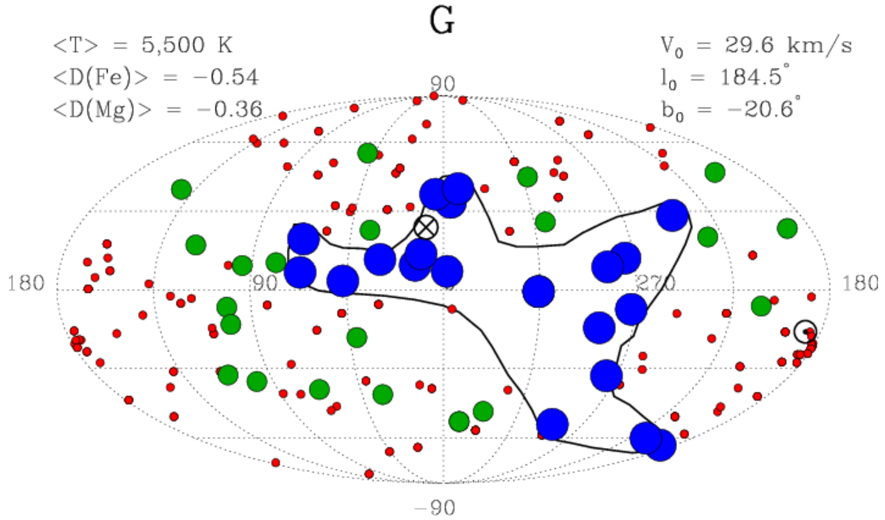

Figure 8. Same as Figure 7 except for the G Cloud.

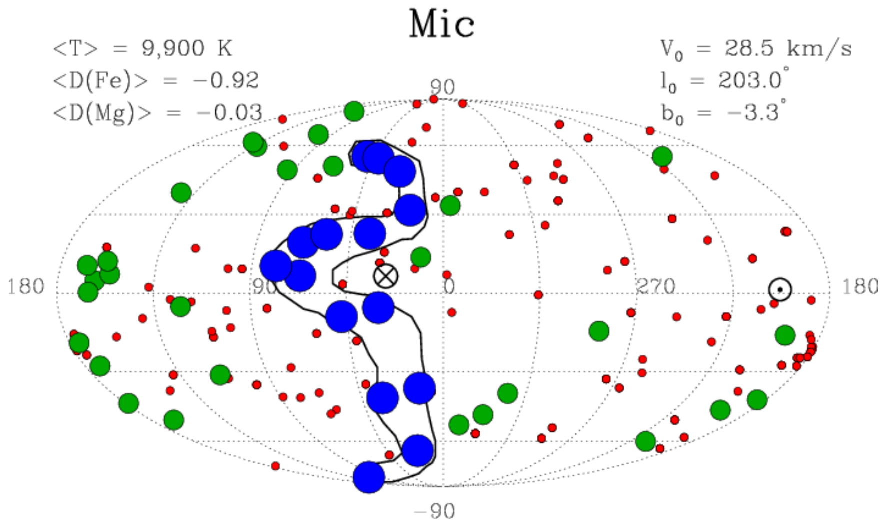

Figure 9. Same as Figure 7 except for the Mic Cloud.

communication) that the scattering screen is only 1.6 ± 1.0 pc from the Sun. Since the location of the turbulent region (l=66°, b=+22°) is at the edge of the two clouds, it is likely that the turbulence is produced by the collision of the G and LIC Clouds, which have a relative velocity of 5.7 km s^{-1}. We will publish a detailed study of this topic in the near future.

Acknowledgements

I wish to thank the FUSE Science Team and Bruce Draine for their collaboration and scientific input concerning deuterium in the Galaxy. I also thank Seth Redfield for his collaboration on the local ISM and Barney Rickett for his input concerning radio scintillation sources. I acknowledge support through grants AR-09525.01A and GO-10236.02 from the Space Telescope Science Institute, which is operated by the Association of Universities for Research in Astronomy, Inc, under NASA contract NAS5-26555.

References

Berghöfer, T.W. & Breitschwerdt, D.: 2002, *Astron. Astrophys.* **390**, 299.
Coc, A., Vangioni-Flan, E., Descouvement, P, & Angulo, C.: 2004, *Astrophys. J.* **600**, 544.
Dennett-Thorpe, J. & de Bruyn, A.G.: 2003, *Astron. Astrophys.* **404**, 113.
Draine, B.T.: 2003, *ARA&A* **41**, 241.
Draine, B.T.: 2006, *ASP Conf. Series* **348**, 58.
Frisch, P.C., Grodnicki, L. & Welty, D.E.: 2002, *Astrophys. J.* **574**, 834.
Geiss, J. & Gloeckler, G.: 2003, *Space Sci. Rev.* **106**, 3.
Heiles, C. & Troland, T.H.: 2003, *Astrophys. J.* **586**, 1067.
Jura, M.: 1982, in Advances in UV Astronomy: 4 Years of IUE Research, ed. Y. Kondo, J.M. Mead, & R.D. Chapman (NASA CP 2238: Greenbelt MD: NASA), 54.
Keller, L.P., Messenger, S., & Bradley, J.P.: 2000, *J. Geophys. Res.* **105**, 10397.
Lallement, R. & Bertin, P.: 1992, *Astron. Astrophys.* **266**, 479.
Linsky, J.L. et al.: 2006, *Astrophys. J.* **647**, 1106.
Linsky, J.L., Diplas, A., Wood, B.E., Brown, A., Ayres, T.R., & Savage, B.D.: 1995, *Astrophys. J.* **451**, 1335.
McKee, C.F. & Ostriker, J.P.: 1977, *Astrophys. J.* **218**, 148.
Meyer, D.M., Lauroesch, J.T., Heiles, C., Peek, J.E.G., & Engelhorn, K.: 2006, *Astrophys. J.* **650**, L67.
Redfield, S. & Linsky, J.L.: 2004, *Astrophys. J.* **613**, 1004.
Redfield, S. & Linsky, J.L.: 2007, in preparation.
Romano, D., Tosi, M., Chiappini, C., & Matteucci, F.: 2006, *MNRAS* **369**, 295.
Romano, D., Tosi, M., Matteucci, F., and Chiappini, C.: 2003, *MNRAS* **346**, 295.
Savage, B.D. & Sembach, K.R.: 1996, *ARA&A* **34**, 279.
Spergel, D.N. et al.: 2003, *Astrophys. J. Suppl.* **148**, 175.
Vázquez-Semadeni, E., Ryu, D., Passot, T., González, R.F., & Gazol, A.: 2006, *Astrophys. J.* **643**, 245.
Wood, B.E., Linsky, J.L., Hébrard, G., Williger, G.M., Moos, H.W., & Blair, W.P.: 2004, *Astrophys. J.* **609**, 838.